ELSEVIER

Available online at www.sciencedirect.com

ScienceDirect

Journal of Nuclear Materials 357 (2006) 31–47

journal of nuclear materials

www.elsevier.com/locate/jnucmat

The effect of annealing at 1500 °C on migration and release of ion implanted silver in CVD silicon carbide

H.J. MacLean [a], R.G. Ballinger [b,*], L.E. Kolaya [c], S.A. Simonson [c], N. Lewis [c], M.E. Hanson [c]

[a] *Idaho National Laboratory, Idaho Falls, Idaho, USA*

[b] *Massachusetts Institute of Technology, Department of Nuclear Science and Engineering, 77 Massachusetts Avenue, Bldg NW-22-117, Cambridge, MA 02139, USA*

[c] *Lockheed Martin Corporation, Schenectady, New York, USA*

Received 20 October 2004; accepted 8 May 2006

Abstract

The transport of silver in CVD β-SiC has been studied using ion implantation. Silver ions were implanted in β-SiC using the ATLAS accelerator facility at the Argonne National Laboratory. Ion beams with energies of 93 and 161 MeV were used to achieve deposition with peak concentrations of approximately 26 wt% at depths of approximately 9 and 13 μm, respectively. As-implanted samples were then annealed at 1500 °C for 210 or 480 h. XPS, SEM, TEM, STEM, and optical methods were used to analyze the material before and after annealing. Silver concentration profiles were determined using XPS before and after annealing. STEM and SEM equipped with quantitative chemical analysis capability were used to more fully characterize the location and morphology of the silver before and after annealing. The results show that, within the uncertainty of measurement techniques, there is no silver migration, via either inter- or intra-granular paths, for the times and temperature studied. Additionally, the silver was observed to phase separate within the SiC after annealing. The results of this work do not support the long held assumption that silver release from CVD SiC, used for gas-reactor coated particle fuel, is dominated by grain boundary diffusion.
© 2006 Elsevier B.V. All rights reserved.

PACS: 61.72.Yx; 61.80.−x; 66.30.−h; 66.30.Jt

1. Introduction

The standard TRISO-coated particle fuel design used for high temperature gas reactor fuel consists of a fuel kernel surrounded by successive layers of: (1) low-density pyrocarbon, (2) high-density pyrocarbon, (3) silicon carbide (SiC) and (4) high-density pyrocarbon. The SiC layer serves as the main barrier to fission product release. Although most fission products, such as cesium, iodine, xenon, and krypton, are retained by the combination of pyrocarbon and SiC layers, previous observations of silver release during fuel testing and operation raises concerns that the SiC layer may not be as effective for

* Corresponding author. Tel.: +1 617 253 5118; fax: +1 617 253 0807.

E-mail address: hvymet@mit.edu (R.G. Ballinger).

0022-3115/$ - see front matter © 2006 Elsevier B.V. All rights reserved.
doi:10.1016/j.jnucmat.2006.05.043

silver. Silver release from SiC coated fuel increases the total activity levels in the primary circuits of high-temperature gas reactors which makes maintenance more difficult and costly.

Silver release has been observed from reportedly or reputed to be intact fuel, suggesting that silver is transported through intact silicon carbide layers. In many cases, experimental measurements of silver release was observed to exhibit a temperature dependence that has been interpreted as a sign of a diffusive mechanism. In most cases, however, silver release has been reported for either a batch of fuel particles or an entire fuel element, leaving uncertainties about individual particle performance. In cases where fission product release from individual particles has been measured, and where individual coated particle characteristics and radiation environments have been essentially identical, silver release, as characterized by rates, timing, and release fractions, has been highly variable. In some cases the release fraction has varied from 0% to 100% among nominally identical particles. This type of behavior is not consistent with a thermally activated process where classical Arrhenius temperature dependence would be expected for all particles.

In previous work, Nabielek et al. implanted low energy silver ions into SiC disk samples at room temperature and measured the concentration profiles before and after annealing [1]. They observed no change in the silver concentration profile after exposure for 30 min at 1180 °C and reported a 'maximum' value for the diffusion coefficient of approximately $1 \times 10^{-19}\ m^2/s$ based on assuming that the actual migration was just below the minimum sensitivity of their detection method. Nabielek et al. attributed their results to silver ions becoming trapped in silicon carbide grains during implantation and not being able to diffuse along grain boundaries.

Although the results of Nabielek et al. were inconclusive, their annealing experiment was conducted at a very low temperature, 1180 °C, with respect to the SiC melting point of 2830 °C and for a very short time. Assuming that a vacancy transport mechanism would be operative one would not expect significant matrix diffusion below approximately half of the absolute melting temperature. Grain boundary diffusion would be of the order 1000× faster than matrix diffusion, but even if this were the transport mechanism the rate would be very slow. For these reasons Nabielek would not be expected to have observed diffusion if a vacancy mechanism were operative. Although there are no directly measured diffusion data for silver reported in the literature in SiC, there are data for other atoms of similar size. Data from Bernhok et al. for aluminum and gallium in 6H–SiC indicate diffusion coefficients in the range 10^{-18}–$5 \times 10^{-16}\ m^2/s$ in the temperature range 1800–2300 °C [2]. Extrapolation of these data to lower temperatures yields values of approximately $10^{-15}\ cm^2/s$ and $10^{-20}\ m^2/s$ at 1500 °C and 1100 °C, respectively. In contrast, reported values of diffusion coefficients, assumed to be grain boundary transport, from silver release measurements have been of the order $10^{-17}\ m^2/s$ and $5 \times 10^{-13}\ m^2/s$ at 1000 °C and 1800 °C, respectively. Thus, there appears to be a significant discrepancy between observed release-based derived diffusion coefficients and what might be expected based on comparison, albeit only approximate, with other similar size atoms, even if grain boundary diffusion is assumed.

Because of the potential significance that a more detailed understanding of the migration of silver in SiC could have for the design of advanced coated particle fuel systems, a program has been under way for the past three years to develop this understanding. Initial results of this program have been reported elsewhere [3,4]. As a part of this program, experimental measurement of the diffusion coefficient of silver in SiC has been a primary goal. Ion implantation experiments have been conducted to investigate silver behavior in SiC at 1500 °C. This temperature was chosen based on the reported literature values for migration of silver in SiC. At this temperature the rates were anticipated to be rapid enough to be easily measured with adequate accuracy. Additionally, this temperature corresponds to the upper operating temperature range for advanced high temperature gas reactor coated particle fuel. These systems make use of SiC as a primary barrier to fission product release. Silver is one of the elements of significant concern for these systems. This paper reports on the results of this program.

2. Experimental

2.1. Materials

Flat plate, CVD SiC, 0.3 cm thick, was the starting material for the ion implantation experiments. The material was obtained from Coorstek, Inc. The reported density was $3.21\ g/cm^3$ with grain sizes in the range of 3–10 μm, preferentially oriented in

the direction perpendicular to the SiC surface. X-ray diffraction (XRD) analysis on a polished SiC sample confirmed that the material was crystalline β-SiC with a strong preferred orientation such that the (1 1 1) planes were parallel to the surface.

Each ion implantation sample was cut to $5 \times 5 \times 0.3$ cm. One 5×5 cm face of each sample was polished to a mirror finish with a mean surface roughness, Ra, of 0.005 μm as measured by a Zygo interference microscope. A flat and uniform initial SiC surface ensured the best possible implanted silver profile.

2.2. Ion implantation

The goal of the ion implantation studies was to implant a measurable quantity of silver in silicon carbide and, moreover, to implant the silver deep enough so that it would not migrate out of the sample during subsequent annealing. Based on silver diffusion coefficients reported in the literature by Amian and Stöver, it was expected that the silver could diffuse farther than 10 μm in as little as 10 h at 1500 °C with the peak concentration dropping to less than 2% of its original value [5]. To prevent excessive silver loss during annealing and to avoid surface effects resulting from the mechanical polishing process, the silver needed to be implanted at a depth of approximately 9–15 μm. Calculations using the SRIM (Stopping and Range of Ions in Matter) code package indicated that ion beam energies on the order of 90–160 MeV were necessary to achieve implantation depths in this range [6].

The silver ion implantation was performed at the ATLAS facility at the Argonne National Laboratory using the positive-ion injector (PII) to create the silver beam. PII consists of three major subsystems: an electron cyclotron resonance (ECR) ion source and high-voltage platform, a 12-MHz beam bunching system, and a 12-MV super conducting LINAC accelerator. The PII ECR source is a 10-GHz electron cyclotron resonance ion source mounted on a high-voltage platform. The beam bunching system compresses the beam into narrow time packets, allowing the LINAC to accelerate the ion beam without introducing significant energy spread. The super conducting resonators in the PII LINAC accelerate the ion beam from the low velocity provided by the PII ECR to the higher velocity required for injection into the remainder of ATLAS.

Two batches of samples were irradiated at ATLAS. The first batch contained samples designated 1, 2a, and 2b. Silver ions with a total energy of 161 MeV and a charge state of +18 were implanted at a mean range of 12.8 μm with a peak at 13.0 μm. The second batch of samples, designated 4a–7b, were implanted with 93 MeV silver ions with charge state +19 at a mean range of 9.05 μm and a peak depth of 9.66 μm. The number of implanted ions ranged from 0.24 to 1.4×10^{17} depending on the run conditions. Table 1 provides the details for the implantation runs.

A copper braid transferred heat from the back of the sample holder to a water-cooled copper block to provide for cooling of the samples during implantation. The temperature at the back of the samples was measured using Type K thermocouples. The measured temperature varied from 120 to 240 °C during the implantation process.

The ion beam consisted of an irregular area approximately 10 mm in diameter with a 4 mm diameter central area where the ion concentration

Table 1
Ion implantation parameters for silver deposition

Sample ID	Beam energy (MeV)	Silver charge state	Irradiation time (h:min)	Time averaged current (eμA)	Minimum current (eμA)	Maximum current (eμA)	Cumulative dose (10^{16} atoms)
1	161	+18	11:43	1.7	1.4	2.2	2.5
2a	161	+18	7:54	2.4	2.3	2.8	2.4
2b	161	+18	22:17	3.2	1.5	4.8	9.3
4a	93	+19	18:31	3.6	2.7	5.1	8.5
4b	93	+19	20:09	5.1	4.1	8.2	13
5a	93	+19	10:10	6.9	7.9	9.8	10
5b	93	+19	9:21	7.6	7.0	9.0	8.7
6a	93	+19	6:27	13.1	12.0	14.0	13
6b	93	+19	6:33	12.4	12.0	13.5	12
7a	93	+19	7:34	10.7	9.8	12.0	13
7b	93	+19	13:21	8.7	7.2	9.8	14

was nearly uniform. The region outside of the central region was much less uniform which resulted in variability in the as-implanted concentration profile. The entire ion beam was used for implantation directly in samples 1, 2a, and 2b. Because of this, the measured depth profiles from these samples were always taken from the center, high concentration area of the implantation. For samples 4a–7b, a mask with a 4 mm diameter hole was used to eliminate the irregular region. The ion implantation process was successful in providing a measurable silver concentration, approximately 2 at.% average and 20 at.% peak, at depths greater than 9 μm with a roughly symmetric concentration profile. This will be discussed further below. Implantation of a high silver concentration ensured that the silver concentration profile would be measurable, above the detection limits of our analysis techniques, both before and after annealing. The beam diameter and depth of the implantation in relation to the initial grain size of the SiC material assured that silver would be present both in the matrix and on grain boundaries.

The purpose of the implantation was to provide a measurable silver distribution at a sufficient depth in the SiC to allow for meaningful annealing experiments. This goal was achieved. The implantation, however, resulted in extensive radiation damage due to the energy loss/displacement cascades developed during the process. It is thus important that questions related to the possible interaction with, and influence of, the damage and silver migration process be addressed. The radiation damage processes resulting from the slowing down of the high energy silver ions can be grouped into two general categories: (1) electronic energy loss and (2) displacement production. As a rule of thumb, the slowing down process is dominated by coulombic interactions (electronic energy loss) until the energy of the ion is reduced to approximately the atomic weight of the stopping atom in keV. Thus, for silver ions, electronic energy loss will dominate until the energy has decreased to approximately 100 keV. Roughly 95–97% of the energy loss will be in the form of heat and the majority of the heat will be deposited in front of where the displacement damage occurs. The remaining energy loss will result in the production of displacement cascades. The displacement cascades produce damage in the form of displacements, dislocation loops, and if the dose and dose rate is high enough, amorphization and/or subsequent crystallization of the material will occur. For the conditions of the implantations in this study, SRIM calculations indicate that significant displacement damage does not begin until a depth of 5 μm and 7 μm is reached for the 93 MeV and 161 MeV cases, respectively. The peak in displacement damage will occur at depths of about 9 μm and 13 μm, respectively. Figs. 1 and 2 show the results of the SRIM calculation for 93 MeV and 161 MeV silver ions in SiC. The SRIM calculations, while using the simplified Kinchen-Pease displacement model gives a relative comparison of the number of displacements and subsequent vacancy production. The calculations are accurate when predicting the energy loss and spatial distribution of damage.

With respect to amorphization, Wendler et al. showed that for high-energy ion damage, amorphization becomes impossible at temperatures above approximately 250 °C [7]. Heera et al. have discussed the dynamic relationship between the damage rate, ion characteristics, and the location of the ion-beam induced epitaxial/amorphized region boundary [8]. Also, Pacaud et al. reported that the crystallization temperature for ion implanted SiC is approximately 950 °C [9]. Based on the results of Wendler [7], Heera [8] and Pacaud et al. [9], it was expected that the implantation process would result in a multi-zone damage region consisting of the following when proceeding from the beam entry point: (1) a region of unaltered SiC where, although the electronic energy loss deposition is very high, the displacement damage will be essentially zero, (2) a region where the displacement damage begins to accumulate which will be severely disrupted, (3) a region where amorphization has occurred since the irradiation temperature was not expected to exceed 250 °C, and (4) a region of undamaged SiC beyond the amorphized region which may have a diffuse boundary due to straggling of the ion slowing down process. The silver is expected to be located in the amorphous region near the boundary away from the beam entry point. With respect to the effect of the radiation damage on the morphology of the silver, as it may affect migration during subsequent annealing, the damage process will result in complete mixing of the SiC and silver in the amorphous region. Since the solubility of silver in SiC is essentially zero, the expected concentrations (~2 at.% averaged over the implantation zone but of the order 20 at.% in the peak deposition zone), would favor precipitation of elemental silver within the damage zone. At the very least, these two processes

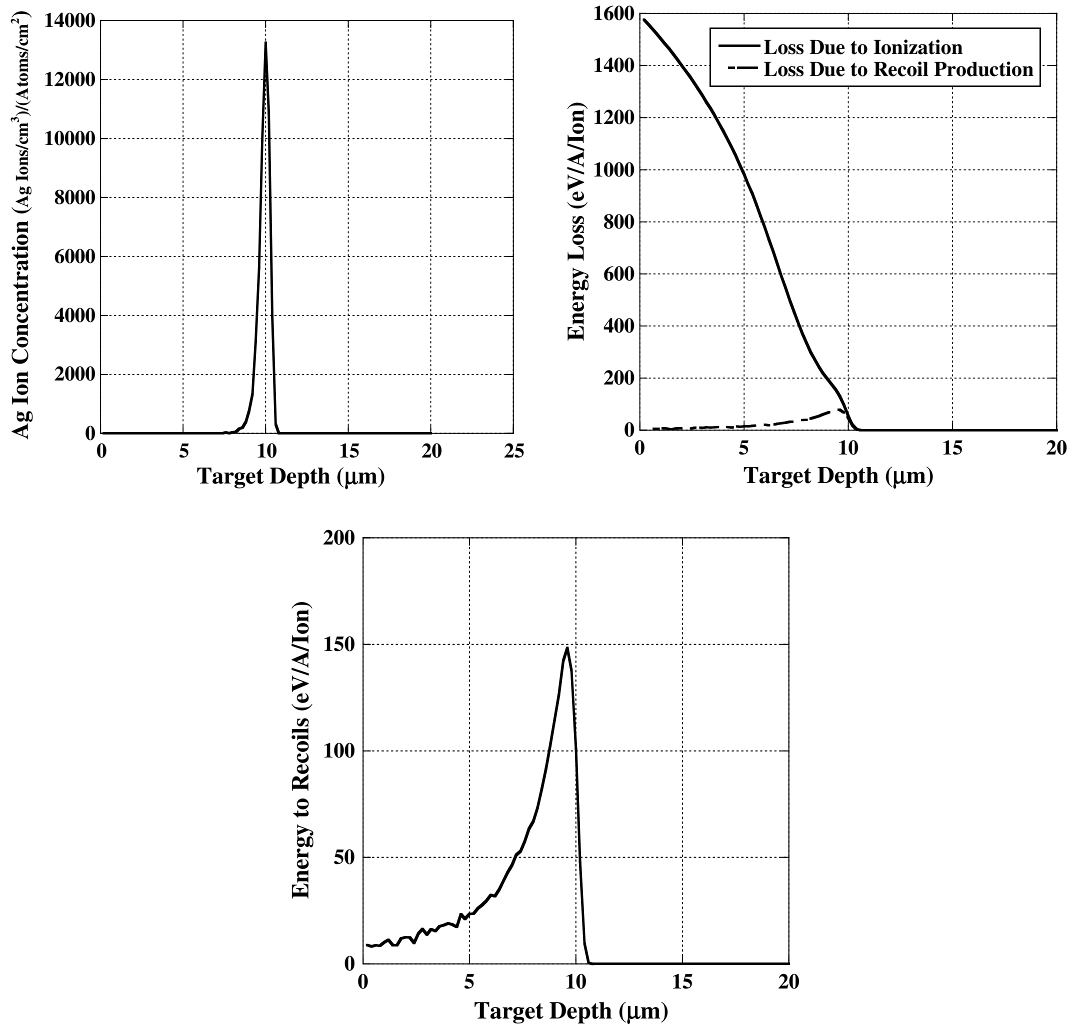

Fig. 1. Results of SRIM calculations for silver implantation at 93 MeV.

would result in silver within grains in the SiC matrix. Additionally, the damage produces an extensive distribution of vacancies. The crystallized region provides grain boundary area for diffusion. Lastly, the annealing process results in crystallization of the amorphous region leading to the production of grain boundaries at the location of the silver. Such conditions should be ideal for migration by diffusion if this occurs. In conclusion, it is expected that the radiation damage from the implantation process would be expected to actually enhance the probability of diffusion.

2.3. Annealing conditions

After implantation, samples were annealed in a graphite furnace at 1500 °C for up to 480 h. This temperature is higher than typical fuel operating temperatures but is in the range of thermal treatments used for previous release-based experiments performed on irradiated fuel. This temperature was also high enough to assure a measurable concentration profile change under the assumption that previously reported diffusion coefficients are accurate. Calculations of the expected profile change based on diffusion coefficients from Amain and Stöver indicated that, even for times of only several hours at 1500 °C, the result would be essentially complete depletion of the silver from the material [5]. Annealing for 210–480 h was, thus, expected to be more than sufficient.

The furnace environment consisted of a moderate vacuum at 1500 °C with typical pressures during annealing in the range of 4–15 mTorr. Each sample

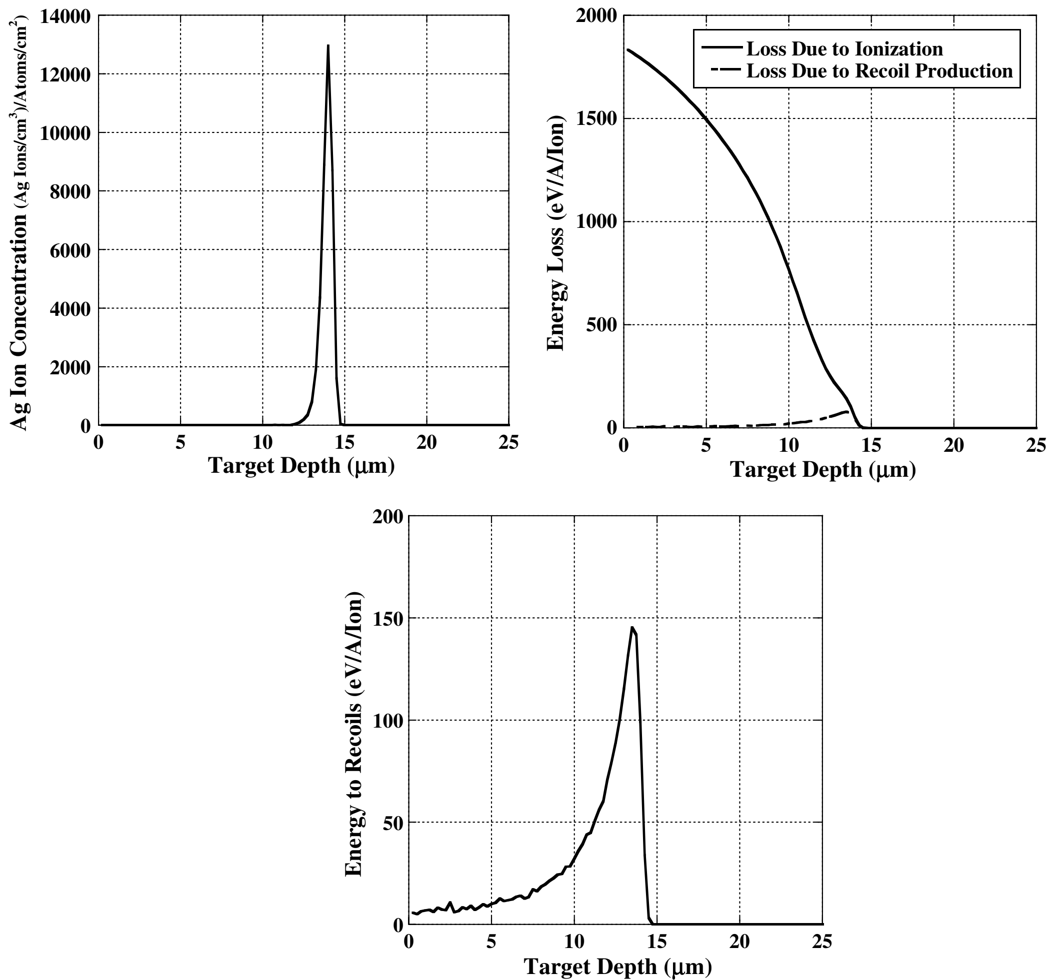

Fig. 2. Results of SRIM calculations for silver implantation at 161 MeV.

was sandwiched between two blocks of silicon carbide, approximately $5 \times 5 \times 1.3$ cm to limit interaction between the surface of the implanted SiC and any contaminants in the furnace atmosphere.

3. Results and discussion

Table 2 shows the experimental parameters and analytical methods for the implantation, annealing, and analysis. Silver concentration profiles were measured in sample 2b before and after annealing at 1500 °C for 210 h. Transmission electron microscopy (TEM) was performed on sample 6a after implantation and sample 5a after annealing for 480 h at 1500 °C to evaluate the effects of implantation and annealing on both the SiC microstructure and the silver distribution.

Table 2
Annealing conditions for selected samples

Sample ID	Implanted dose (atoms/cm^3 @ MeV)	Temperature (°C)	Time (h)	Analysis
2b	1.9E+21 (161 MeV)	1500	210	XPS profile
5a	2.1E+21 (93 MeV)	1500	480	TEM
6a	2.6E+21 (93 MeV)	n/a	n/a	TEM

3.1. Silver concentration profiles

Fig. 3 shows the results of X-ray photoelectron spectroscopy (XPS) profile measurements before and after annealing at 1500 °C for 210 h. The best estimate of the errors in both position and concentration are indicated with error bars, which will be discussed below. Within the accuracy of the measurements there is no significant change in the profile after annealing.

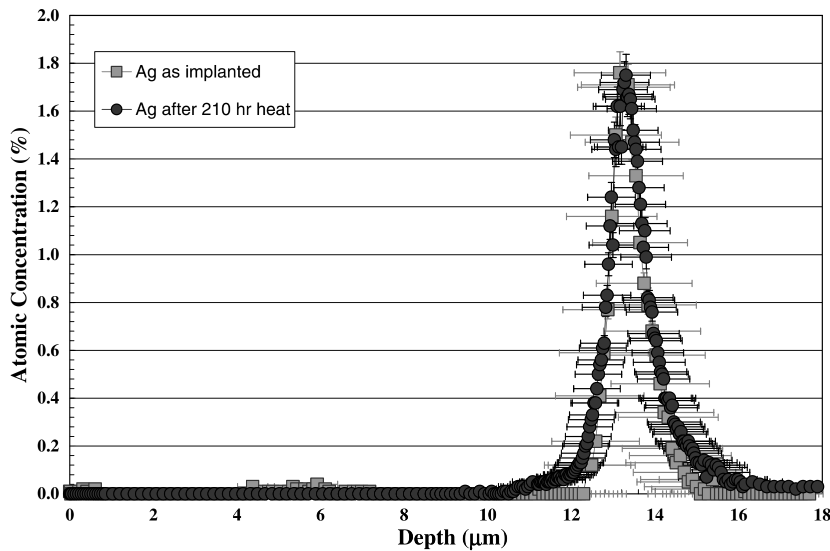

Fig. 3. Silver concentration profiles in sample 2b before and after annealing.

3.2. Sources of uncertainty

Uncertainty in the concentration profile analysis can be grouped into two major categories: (1) that derived from uncertainty in the spatial location of the analysis and the geometry of the sputter crater, and (2) uncertainty in the measured chemical composition due to simple counting statistics. Uncertainties in spatial location arise from uncertainties in the sputtering rate for the XPS system. No standard was available for calibration of the sputtering rate for SiC. However, after analysis the sputter time/depth correlation was verified by actual measurements. Uncertainties in the measured chemical compositions were derived from counting statistics, the efficiency of the analysis for a particular element and a complex interaction between depth uncertainty and shielding due to non-ideal sputter crater shape.

To achieve the best comparison between silver concentration profiles before and after annealing, it was necessary to use the same sample for each analysis. To accomplish this, a gold foil containing a 1.3 mm diameter hole was placed over the implanted region for the pre and post-annealing concentration profile determination to localize the sputter crater for each analysis. The XPS depth profile analysis consisted of a sequence of chemical analyses followed by sputtering of the surface to remove material. After sputtering the next chemical analysis was performed. The gold foil mask served to localize both the chemical analysis and the sputtering area. After annealing, a region far enough away from the pre-annealing analysis region, yet still within the uniform implantation region, was used for the post-annealing analysis. Although the use of a mask facilitated the before and after annealing analysis it introduced additional uncertainty in the chemical analysis, both in the calculated concentration and in the spatial location of the analytical volume. The source of this uncertainty included self-shielding during sputtering which leads to edge rounding of the sputter crater. An uneven and sloped crater bottom also increased the uncertainty of the total depth of the crater. Additionally, the restriction of the size of the sputter area increased uncertainty in the final concentration profile. The bottom of the sputter crater was less than the diameter of the mask hole. The irradiated volume at a particular depth, therefore, included signal from a depth region which included both the bottom of the sputter crater as well as the rounded shoulders of the sputter crater. In addition, signal was likely derived from scattering and interaction between the analysis beam and the sides of the sputter crater. Analysis of these factors yielded an estimate that up to 10% of the data signal actually came from the rounded edges of the sputter crater and from the side walls of the sputter crater.

As was mentioned earlier, a silicon carbide sputter standard was not available to determine the sputter rate during the XPS analysis. A calibration

was developed, however, by using a Zygo interference microscope to measure the depth and shape of the sputter craters after analysis. The depth of the sputter craters was then used to calculate the sputter rate. The sputter rate was assumed constant throughout the silicon carbide and equal to the total crater depth divided by the total sputter time. An uneven and sloped crater bottom, however, introduced uncertainty in the total depth of the sputter crater and, hence, the sputter rate.

Although uncertainties in the silver concentration profile tend to artificially widen the measured concentration profile, they are present in both the before and after annealing analyses. Thus, although there will be uncertainty in depth, this will be at least partially compensated for by the fact that both before and after annealing analyses were performed in exactly the same way.

Fig. 3 includes the effect of uncertainties shown as error bars in both the position and the chemical analysis. The error bars shown in Fig. 3 represent the best estimates by the authors. However, while reasonable estimates for the spatial and counting statistics related errors could be obtained, the effect of shielding could only be characterized qualitatively. Within the uncertainty of the XPS analysis, there was no silver migration during annealing.

3.3. Electron microscopy

3.3.1. Introduction

Electron microscopy was used to characterize the SiC microstructure before and after annealing and the location of the implanted silver. Thin cross-sectional slices of two ion implantation samples, one before annealing and one after, were analyzed using scanning electron microcopy (SEM) and analytical electron microscopy (AEM).

The goal of the AEM analysis was to observe and characterize the silver location and morphology in the implanted region, both before and after annealing. An additional goal was to characterize the silicon carbide grain structure both within and outside the implantation region and also to characterize, if possible, the damage in the implanted region. The results of this analysis are shown in Figs. 4–9 and discussed in the following sections.

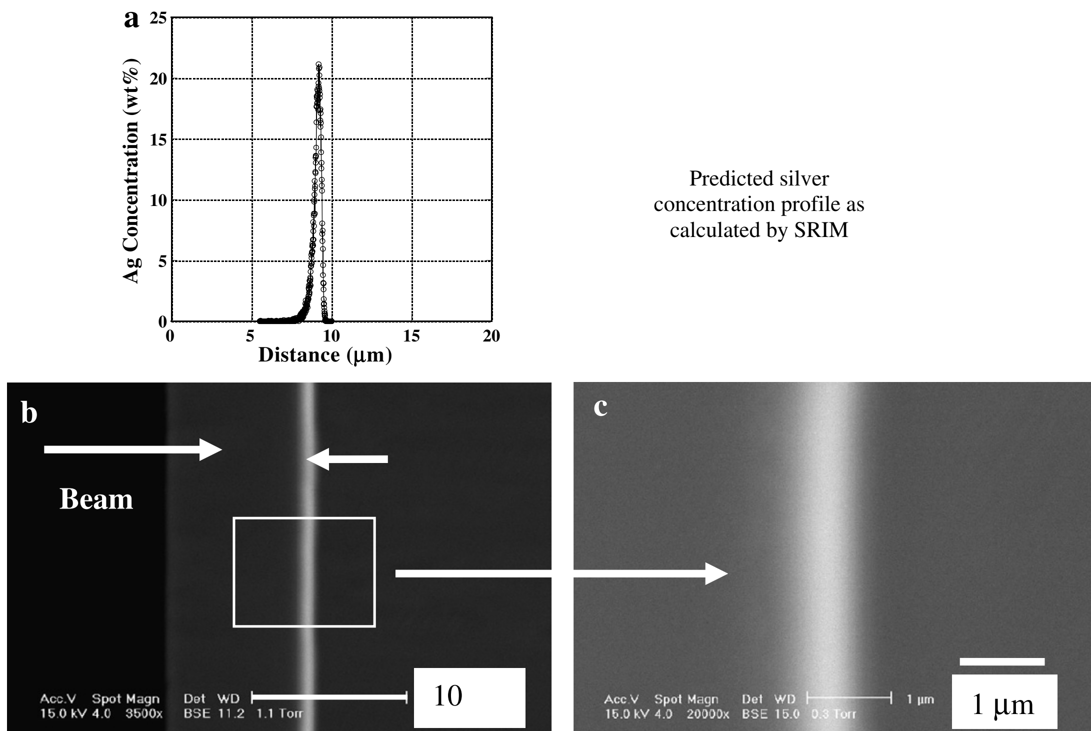

Fig. 4. SEM micrographs showing as-implanted silver location in SiC.

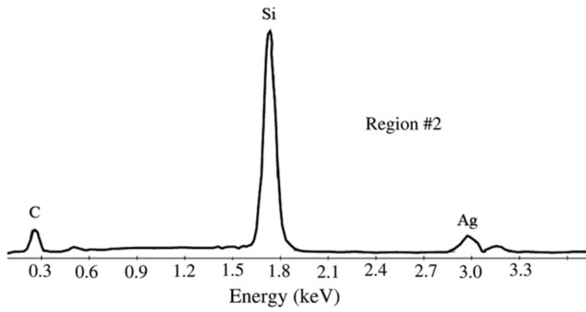

Fig. 5. EDS spectra for as-implanted material. Silver is concentrated within a narrow band corresponding to the region predicted by SRIM calculations.

3.3.2. As-implanted microstructure

Fig. 4 shows back scatter SEM micrographs of the as-implanted (sample 6a) material. Fig. 4(a) shows the SRIM calculated silver profile. Fig. 4(b) and (c) shows the as-implanted microstructure at low and high magnification. The light region is the area of high silver concentration. Fig. 5 shows energy dispersive X-ray spectroscopy (EDS) results for the region labeled 2 in Fig. 4(b). No silver was detected in the regions labeled 1 or 3 in Fig. 4. The location of the silver is consistent with the calculated displacement damage morphology shown in Figs. 1 and 2.

Fig. 6 shows an analytical electron micrograph (AEM) of the as-implanted SiC microstructure prior to annealing. The silver ion beam entered from the left. The as-implanted microstructure consists of a zone of altered SiC sandwiched between regions of apparently unaltered material. The altered microstructure region, however, does not completely define the extent of the implantation-induced damage. As Figs. 1 and 2 show, the damage zone extends from the entry point of the ion beam to a short distance beyond the inner-most extent of the zone of microstructural change. The region of vacancy production, although peaked in the region of highest displacement damage, would encompass the entire region. Also, although the displacement damage zone is skewed to the right, the electronic energy loss region is skewed to the left side of the region. Thus, the region of peak heat generation rate would also be skewed to the left side of the zone.

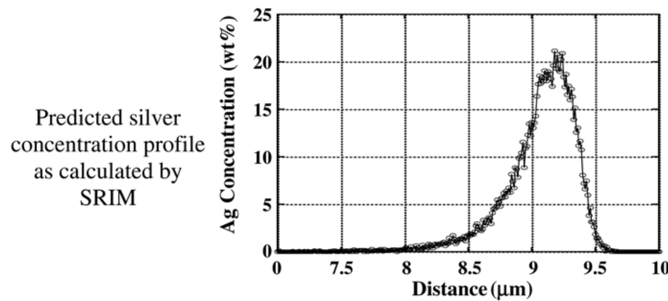

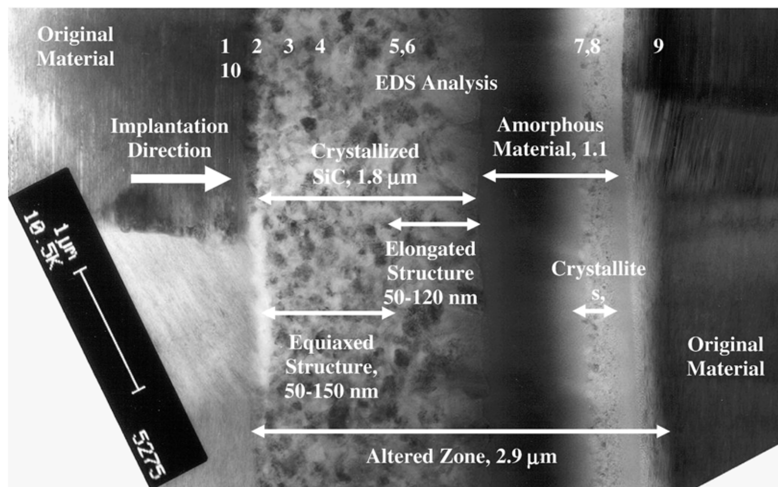

Fig. 6. AEM micrograph of as-implanted SiC before heating.

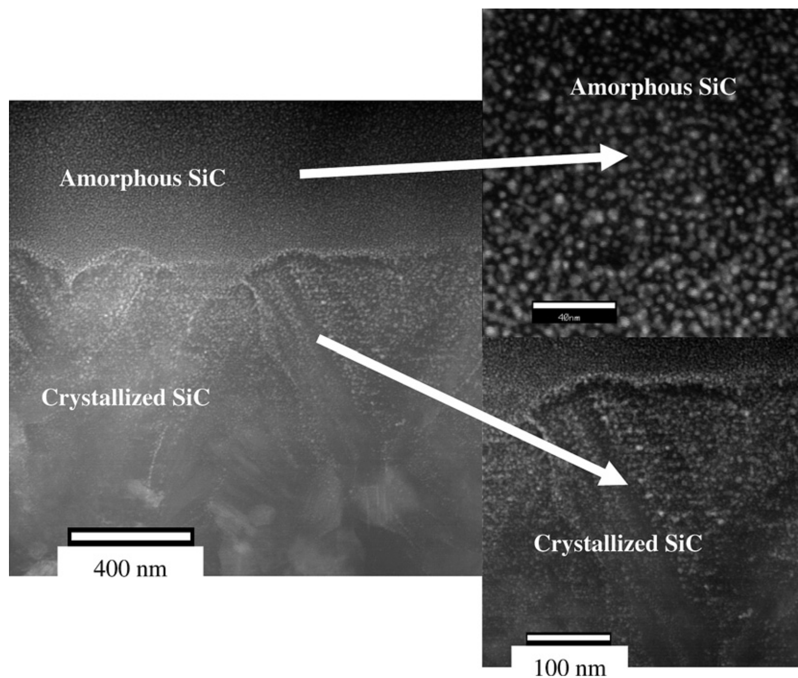

Fig. 7. STEM micrographs of as-implanted SiC showing the region at the interface between the amorphous and crystallized regions.

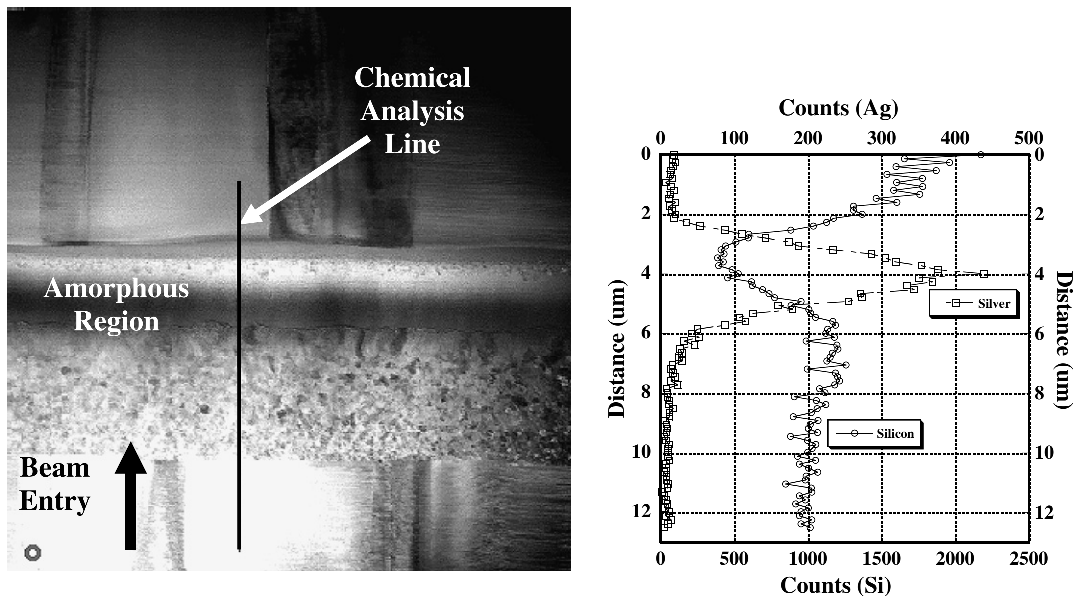

Fig. 8. STEM analysis for silicon and silver. The silver concentration peaks in the amorphous region.

In the as-implanted microstructure, a crystallized region defines the front of the silver implantation zone. The as-fabricated silicon carbide columnar grain structure is visible to the left and right of the altered zone. The altered zone consists of three main regions. In the front-most region of the implantation zone, on the left, crystallization has occurred. The middle of the altered zone contains an amorphous region. Towards the back, the structure is still mostly amorphous, but small crystallites have nucleated.

Although the morphology of the crystallized region at the front of the implantation zone is

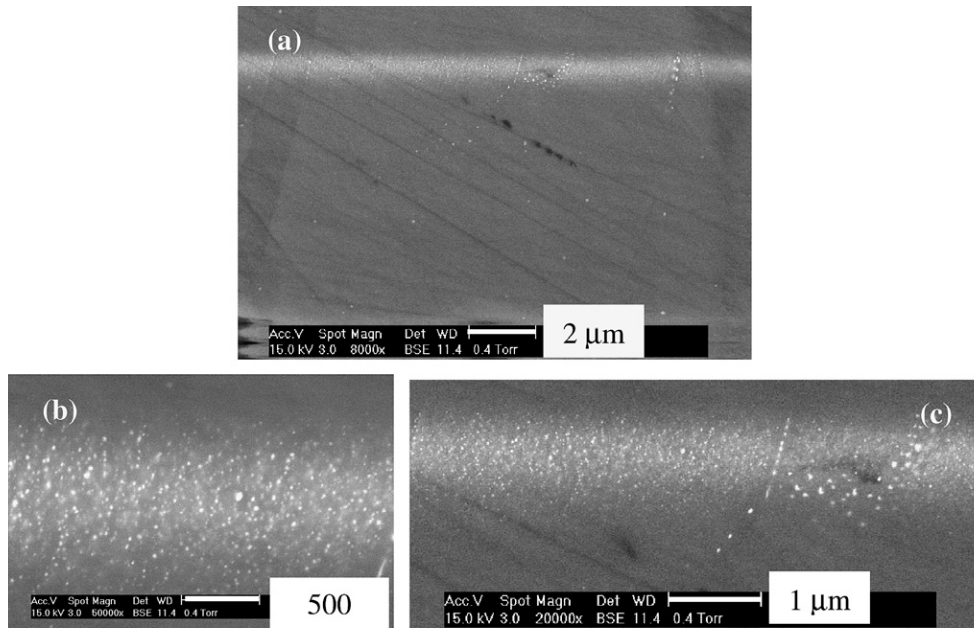

Fig. 9. SEM back scatter image of the annealed microstructure.

fine-grained and equiaxed, there appears to be a further distinction between smaller, more equiaxed grains at the front and slightly larger, more elongated grains at the back. The smaller equiaxed grains are on the order of 50–150 nm in diameter and the larger grains are about 100–200 nm wide by 250–400 nm long.

The back 1.1 μm of the altered zone is largely amorphous, but also contains some small equiaxed crystallites ranging in size from less than 4 nm to about 30 nm in diameter. SiC grains have nucleated and started to grow in the rear of the amorphous region during implantation, but have not been able to incorporate all of the material. A thin band of the as-fabricated SiC behind the altered zone, about 300–400 nm wide, contains damage with increased faulting, though the damage was not great enough to cause amorphization or crystallization.

Chemical analyses, using EDS, were performed along the cross-section of the implanted sample to provide a quantitative assessment, on a macro scale, of the silver concentration. The locations of EDS measurements are identified in Fig. 6 and the silver concentrations are listed in Table 3. The silver profile agrees with the predicted silver implantation profile. No silver was observed in the original material in front of the altered zone or in the front portion of the recrystallized zone. Silver just above the detection limit of 1000 ppm (0.1 at.%) was measured in the recrystallized zone at the boundary between the equiaxed and slightly columnar SiC grains. The peak silver concentration occurs in the amorphous region. A small amount of silver was detected at the boundary between the amorphous region and the original SiC as well as in the damaged layer of the original SiC just behind the altered zone.

Table 3
Silver concentration in the as-implanted SiC as a function of location-referenced to the locations identified in Fig. 6

Spot #	Location	Relative silver concentration*
1	Original SiC, Front	None detected
2	Interface between front SiC and recrystallized SiC	None detected
3	~0.2 μM into recrystallized SiC	None detected
4	In the middle of the recrystallized, equiaxed SiC	1.1
5	Between the equiaxed and	2.8
6	Columnar recrystallized SiC	5.1
7		26.3
8	Amorphous damaged region	25.1
9	Interface between amorphous SiC and original SiC	4.0
10	Damage zone of original SiC	1.2

* Silver concentration in wt%. Spot # identified in Fig. 6.

In addition to the AEM analysis, the as-implanted microstructure was analyzed using scanning transmission electron microscopy (STEM).

The analysis was performed using a Vacuum Generators HB601 STEM at an acceleration voltage of 250 kV. The STEM allows for analysis at very high resolution. Fig. 7 shows the morphology at the interface between the amorphous and recrystallized regions and Fig. 8 shows the results of microchemical analysis for silver through the implanted region.

At this resolution the silver morphology depends on the specific region within the altered zone. In the amorphous region the silver is separated into small, approximately 5 nm diameter, regions. The distribution of these regions is random, in keeping with the amorphous nature of the SiC. In the crystallized material the silver particle size is slightly larger but the morphology is oriented within the crystal structure. β-SiC (3C–SiC) crystallizes in the zinc blende structure that can be visualized as two interconnecting (carbon and silicon) face centered cubic lattices. The morphology of the silver suggests a preference for precipitation on the close packed planes in this structure. Fig. 8 shows an elemental line scan through the amorphous region generated using the STEM. The results, although qualitative, confirm that the silver is located primarily within the amorphous region.

3.3.3. Annealed microstructure

Figs. 9–14 show the microstructure of the annealed (480 h at 1500 °C) material. Fig. 9 shows a set of SEM back scatter images at increasing magnification. A comparison of Fig. 9 with Fig. 4 shows that the morphology of the silver coarsened during the anneal. Moreover, it appears that preferential precipitation has occurred in some regions as the brighter localized regions in the right side of Fig. 9a show. Fig. 10 shows a STEM micrograph and silver map for the annealed material. The silver has remained segregated within the implanted region.

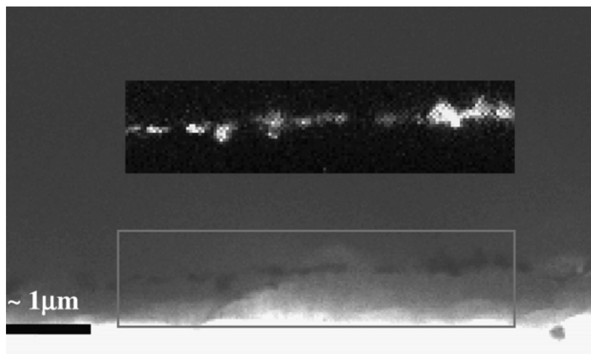

Fig. 10. STEM micrograph with silver element map showing silver location after annealing at 1500 °C for 480 h.

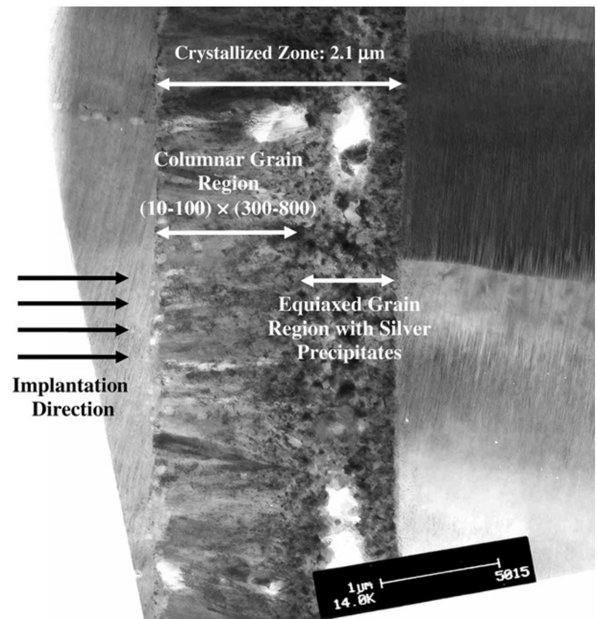

Fig. 11. TEM micrograph of as-annealed material after 480 h @ 1500 °C.

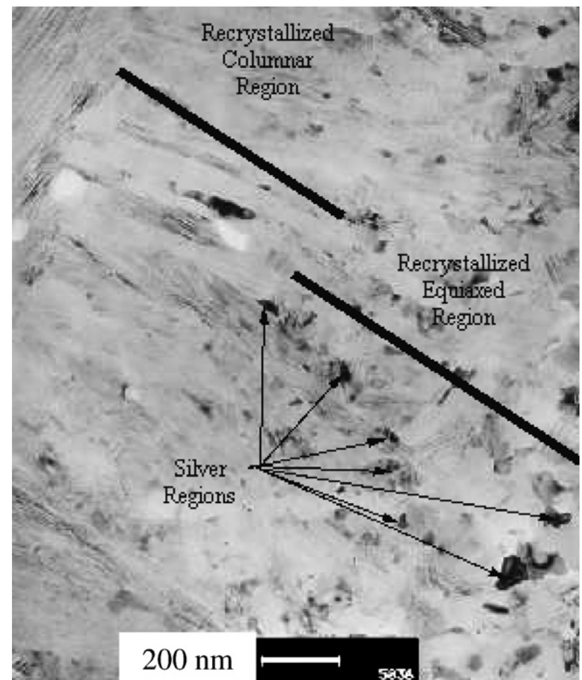

Fig. 12. Detail of crystallized region after annealing showing typical areas where silver was detected.

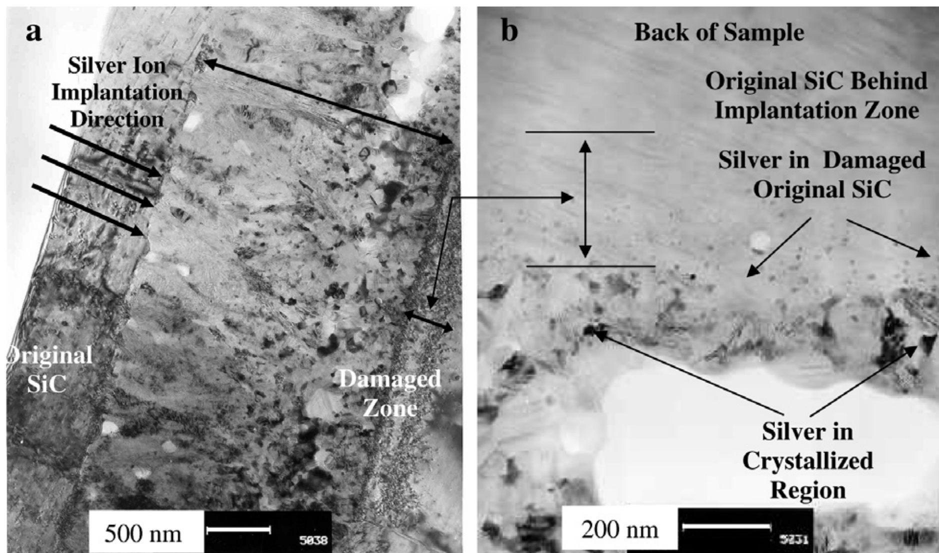

Fig. 13. AEM micrograph series of annealed material showing details of region behind the crystallized region.

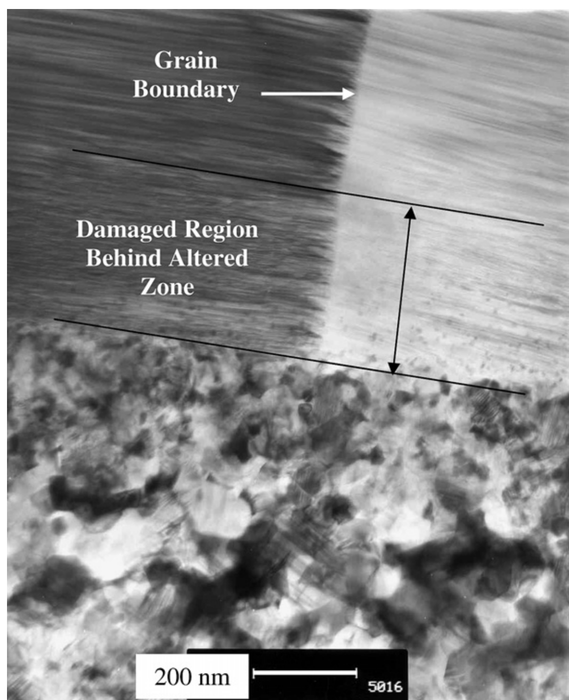

Fig. 14. AEM micrograph showing details of a SiC grain boundary at the interface between damaged and undamaged regions after annealing for 480 h at 1500 °C. No silver could be detected on grain boundaries.

Figs. 11–13 show TEM micrographs of the annealed microstructure. Fig. 11 shows the microstructure of the entire implanted region. The implantation zone completely crystallized, as expected. This is shown more clearly in Fig. 12. The amorphous SiC was completely eliminated in the altered zone after annealing. The crystallized zone is approximately 2.1 μm wide and is characterized by two regions. The front region, which closely corresponds to the region formally crystallized during the implantation process, has been transformed into an epitaxial, columnar region. The formally amorphous region has crystallized and is characterized by a fine equiaxed structure. The back half of the crystallized zone also contains precipitated silver regions, phase separated from the silicon carbide. The silver appears darker than the SiC due to its higher atomic number. The silver is segregated from the SiC and has accumulated between grain boundaries.

Figs. 13 and 14 show TEM micrographs of the annealed microstructure, focusing on the area immediately behind the crystallized region. In this region, the implantation damage was not sufficient to cause amorphization of the original microstructure. Radiation damage calculations, however, indicate that displacement damage should have been present. Small precipitates of silver decorate the silicon carbide behind the crystallized zone. These silver precipitates are approximately 4–20 nm in size. The layer is approximately 300–400 nm wide. Silver is only present in the damaged region and does not appear in the undamaged, as-deposited SiC. Fig. 14 shows the details of a typical grain boundary

region. Extensive analysis of the grain boundaries in the region immediately behind the damaged region, where grain boundaries from the undamaged region intersect the damaged, silver-containing region, did not detect the presence of silver. Silver was not observed in the undamaged SiC regions.

4. Discussion

4.1. Comparison of as-implanted and annealed behavior

The implantation process resulted in the creation of both crystalline and amorphous regions in the CVD SiC microstructure. At the concentrations implanted in this study, approximately 2 at.% averaged, the observation of phase separated silver over a very narrow damaged region was not unexpected. Nevertheless, from the standpoint of establishing the initial conditions for the study of migration of silver in SiC, this process achieved its goal. The as-implanted microstructure contained silver in intimate contact with the SiC both in the matrix and in immediate proximity to grain boundaries.

The crystallization process created new grain boundaries as well as a significant increase in grain boundary area relative to the original CVD SiC microstructure. As the amorphous SiC crystallized to form β-phase grains, impurity silver atoms were rejected due to their low solubility. The change in morphology of the silver is clearly evident in the SEM micrographs in Figs. 7 and 9. The silver atoms segregated from the crystallized SiC grains and continued to appear as phase-separated precipitates in the crystallized zone. During the annealing process the silver had access to the SiC grain boundaries, however, no silver migration was observed either by XPS or AEM analyses. A region of low-concentration silver exists just behind the crystallized SiC in the heavily faulted original SiC microstructure yet, there is no evidence of silver migration along grain boundaries present in the original SiC. If grain boundary diffusion is the most likely mode of migration, it should have been evident in this region.

With respect to the question of the effect of radiation damage on potential introduction of 'artifacts' that would influence the diffusion process, consider the shape of the concentration profile before and after annealing. If there was a significant influence of radiation damage on the subsequent high temperature diffusion process, the supersaturation of vacancies that would have existed as a result of the implantation process should have provided for enhanced diffusion in the damaged region but not in the undamaged region. Rough calculations indicate that the vacancy production rate in the peak damage region would have been of the order 10^{21} vacancies/s/cm^3. The vacancy production rate would have tailed off toward the beam entry region but would still have been significant. The vacancy production rate, however, would have tailed off much more abruptly beyond the peak damage region and would have been zero in the region beyond the damaged region. Since the implantation temperature was far below any temperature for which vacancy migration would have been significant, the vacancy concentration would have been very high prior to annealing.

4.2. Comparison to literature

In a previously reported ion implantation experiment, Nabielek et al. did not observe silver diffusion. Nabielek et al. implanted lower energy silver ions into silicon carbide at room temperature, just below the surface, and annealed the sample for only 30 min at 1180 °C [1]. Rutherford backscattering measurements before and after annealing showed no change in the silver concentration profile. The authors concluded that silver had most likely been trapped in SiC grains and, therefore, silver diffusion was not observed because matrix diffusion of silver in SiC is much, much slower than grain boundary diffusion. Early results from this research program have also indicated that migration by diffusion does not occur [3,4]. Recent results from Jiang et al., who implanted 6H–SiC with 2 MeV Si ions followed by annealing at 1300 °C, support this observation [10].

The results of this work suggest that, while trapping of some silver in the SiC matrix may be occurring, immobilization of silver at SiC grain boundaries is also likely occurring. The solubility of silver in silicon carbide is extremely low, as these results confirm, and silver was swept from the grains during crystallization yet no change in the shape of the concentration profile was observed.

In another study of the retention of silver in coated particle fuel, Nabielek observed (as have others) a large variability in the retention of silver for nominally identical conditions [11]. He postulated that one possible explanation for the observed behavior is that migration of silver is enhanced by the presence of free silicon on the grain boundaries. No evidence was offered to support this hypothesis.

Table 4
Silver release data from Ref. [14]

Test ID reference	Irradiation time (effective full power days)	Temperature (°C)	Burnup (% FIMA)	Ag^{110m} release fraction
HFR-K3/2	359	920	10	0.00045
HFR-K3/3	359	920	10.6	0.00016
FRJ2-K15/1	533	970	14.1	0.00075
R2-K13/4	517	980	9.8	0.0027
FRJ2-P27/1	232	1080	7.6	0.018
R2-K12/1	308	1100	11.1	0.033
FRJ2-K13/4	396	1120	7.6	0.039
FRJ2-K13/1	396	1125	7.5	0.019
FRJ2-P27/3	232	1130	7.6	0.020
FRJ2-K13/2	396	1150	8	0.020
FRJ12-K13/3	396	1150	7.9	0.017
FRJ2-K15/2	533	1150	15.3	0.0032
R2-K13/1	517	1170	10.2	0.039
HFR-K3/1	359	1200	7.5	0.0022
HFR-K3/4	359	1220	9	0.018
R2-K12/2	308	1280	12.4	0.014
FRJ2-P27/2	232	1320	8	0.0082

XPS results from this work did not show the presence of free silicon although the sensitivity of the analysis was only approximately 0.1 at.% for free silicon.

Another possibility for a rationalization of the difference between release-based diffusion measurements, their high variability, and the results of this work might be that the release is due to an entirely different mechanism. One mechanism could be vapor transport through 'nano' cracks that are either present from the fabrication or are generated during thermal and irradiation exposure or surface diffusion along the surfaces within these cracks. Recent results using specially prepared spherical diffusion couples, where the silver was encapsulated within a sphere of SiC, appear to show the same variability in release that has been observed with actual fuel particles [12]. To the accuracy of the chemical analysis performed to date, no silver has been observed within the SiC after annealing in the 1200–1700 °C temperature range. Additionally, helium leak testing of samples before and after heating has shown an increase in leak rates [12]. Since helium leaks can only occur if mechanical paths are present, this gives support to the possibility that vapor transport may be playing a role. Additional support for the vapor transport hypothesis is provided by an analysis of silver release data from several experiments at different irradiation temperatures presented by Nabielek et al. [14]. These data are shown in Table 4 and plotted in Fig. 16. If vapor transport plays a significant role in the release process then there should be a precipitous drop in release when the temperature drops below the melting point of silver. The data compiled by Nabielek et al. [14] appears to show this.

Also important to note is that the final crystallized SiC grain structure for the results reported here is similar to that fabricated in typical SiC layers in tested TRISO-coated particle fuel. Although there are differences between some of the coating

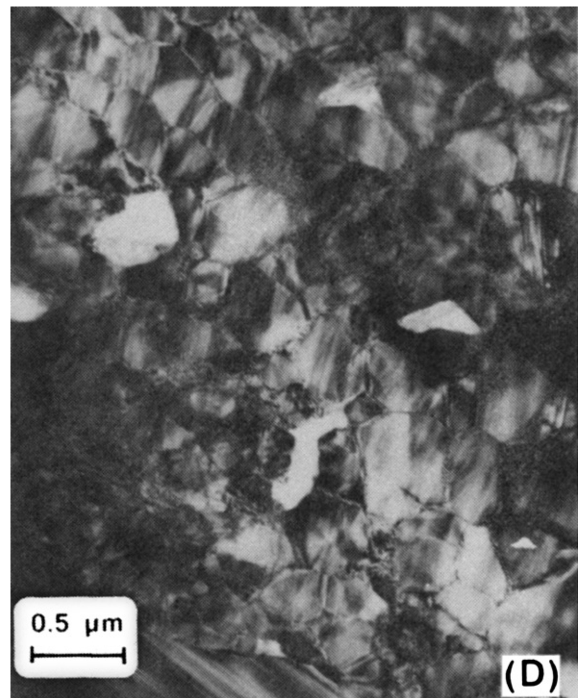

Fig. 15. Comparison of typical CVD SiC microstructures [13].

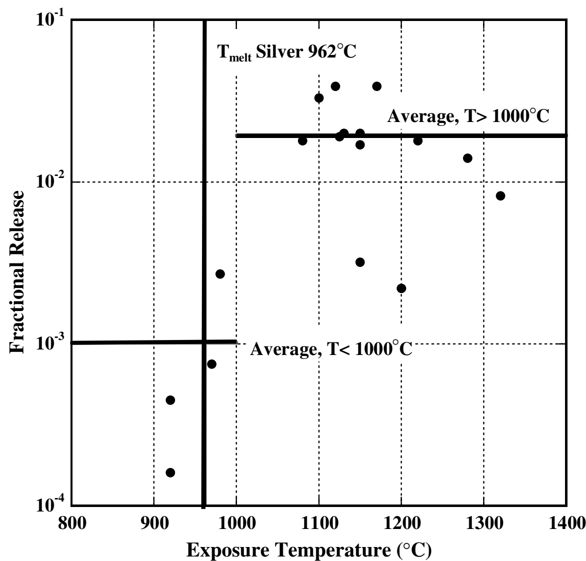

Fig. 16. Silver fractional release vs. exposure temperature. Data points from Ref. [14].

parameters, the SiC used in this work and the SiC from previous fuel tests were coated using the same high temperature CVD process which resulted in high-density β-SiC with a fine-grain structure. Fig. 15 shows the microstructure that is typical of TRISO-coated SiC fuel [13]. This microstructure should be compared with the equiaxed microstructure shown in Fig. 14. The two microstructures are quite similar. This similarity suggests that these results have applicability to the case where silver release is occurring in TRISO-coated particle fuel.

5. Conclusions and implications

The results of this work show that silver did not measurably move by diffusion, either in the matrix or along grain boundaries, in SiC for the conditions studied and within the accuracy of our measurements. For migration by diffusion to still be occurring but at concentrations just below the minimum sensitivity of our analysis, the average diffusion coefficient would have to be less than 5×10^{-21} m^2/s.

The silver concentration used in this work is well above that which would be expected to exist in TRISO-coated particle fuel. The annealing temperature for this work, however, is in the same range as the post-irradiation annealing studies used to derive diffusion coefficients for coated particle fuel. Additionally, the microstructure of the SiC used in this work is either similar to TRISO-coated particle fuel SiC or of a structure that should have enhanced the resulting silver migration behavior. We thus conclude that these results have applicability to the case of silver migration in CVD SiC for coated particle fuel.

The results of this work indicate approaches that might be applied to the mitigation of silver release in coated particle fuel. If, as has been previously assumed, release is by diffusion then little can (or could) be done to mitigate release short of changing to a more resistant material. However, if silver does not diffuse in silicon carbide, then silver release from coated particle fuel must be controlled by transport along another path. These results indicate that the path may be more mechanical then microstructural although it is likely that microstructure would play a critical role in allowing mechanical paths to develop. However, under these circumstances additional work may both identify the actual path and then point to ways of reducing the probability of this path from developing.

Acknowledgements

The authors appreciate the analysis provided by Jim McGee, Paul Sander, Gerry Neugebauer, and John Azarkevich of Lockheed Martin. Richard Pardo and Rick Vondrasek provided support and guidance for the silver ion implantation at ATLAS. Timothy Antaya at the Massachusetts Institute of Technology was instrumental in contacting implantation facilities and guiding the initial design of the ion implantation rig. The research was conducted as part of a DOE I-NERI project. The authors are also grateful for the comments and suggestions provided by Heinz Nabielek, and Forschungszentrum Julich, Bill Morris at ORNL, and Carl McHargue at the University of Tennessee.

References

[1] H. Nabielek, P.E. Brown, P. Offerman, Nucl. Technol. 35 (1977) 483.
[2] J. Bernhok, S.A. Kajihara, C. Wang, A. Antonelli, R.F. Davis, Mater. Sci. Eng. B 11 (1992) 265.
[3] H.J. MacLean, R.G. Ballinger, Silver migration and release in thin silicon carbide, ANS Annual Winter Meeting, Washington, DC, November 2002.
[4] H.J. MacLean, R.G. Ballinger, Silver migration in SiC: a new perspective, ANS Global 2003, New Orleans, LA, 17–20 November 2003.
[5] W. Amian, D. Stöver, Nucl. Technol. 61 (1983) 475.

[6] J.F. Ziegler, J.P. Biersack, The Stopping and Range of Ions in Matter (SRIM). Available from: <www.SRIM.org>, Copyright (1984, 1986, 1989, 1994, 1998, 2003).
[7] E. Wendler, A. Heft, W. Wesch, Nucl. Instrum. and Meth. B 141 (1998) 105.
[8] V. Heera, T. Henkel, R. Kogler, W. Skoroupa, Phys. Rev. B 52 (1995) 776.
[9] Y. Pacaud, J. Stoemenos, G. Brauer, R.A. Yankov, V. Heera, M. Voelskow, R. Kogler, W. Skorupa, Nucl. Instrum. and Meth. B 120 (1996) 177.
[10] W. Jiang, W.J. Weber, V. Shutthanadan, L. Li, S. Thevuthasan, Nucl. Instrum. and Meth. B 219 (2004) 642.
[11] H. Nabielek, The mechanism of silver retention in coated particle fuel, DPTN/801, OECD High Temperature Reactor Project, Kernforschungsanlage Julich, A.E.E. Winfrith, Dorchester, Dorset, England, April 1976.
[12] H.J. MacLean, Silver Transport in CVD Silicon Carbide, Ph.D. Thesis, MIT, Department of Nuclear Engineering, June 2004.
[13] C.H. Carter Jr., R.F. Davis, J. Bentley, J. Am. Ceram. Soc. 67 (1984) 732.
[14] H. Nabielek, D. Goodin, W. Scheffel, Criteria for a high performance particle, HTR-TH International HTR Fuel Seminar, Brussels, Belgium, 1–2 February 2001.